Influenza-Induced Oxidative Stress Sensitizes Lung Cells to Bacterial-Toxin-Mediated Necroptosis

Norberto Gonzalez-Juarbe[1,5,6,*], **Ashleigh N. Riegler**[1], **Alexander S. Jureka**[2], **Ryan P. Gilley**[3], **Jeffrey D. Brand**[4], **John E. Trombley**[4], **Ninecia R. Scott**[1], **Maryann P. Platt**[5], **Peter H. Dube**[3], **Chad M. Petit**[2], **Kevin S. Harrod**[4], **Carlos J. Orihuela**[1]

[1]Department of Microbiology, The University of Alabama at Birmingham, Birmingham, AL 35294-2170, USA

[2]Department of Biochemistry and Molecular Genetics, The University of Alabama at Birmingham, Birmingham, AL 35294-2170, USA

[3]Department of Microbiology, Immunology and Molecular Genetics, The University of Texas Health Science Center at San Antonio, San Antonio, TX 78229, USA

[4]Department of Anesthesiology and Perioperative Medicine, The University of Alabama at Birmingham, Birmingham, AL 35294-2170, USA

[5]Infectious Diseases and Genomic Medicine Group, J Craig Venter Institute, 9605 Medical Center Drive, Suite 150, Rockville, MD 20850, USA

[6]Lead Contact

SUMMARY

Pneumonias caused by influenza A virus (IAV) co- and secondary bacterial infections are characterized by their severity and high mortality rate. Previously, we have shown that bacterial pore-forming toxin (PFT)-mediated necroptosis is a key driver of acute lung injury during bacterial pneumonia. Here, we evaluate the impact of IAV on PFT-induced acute lung injury during co- and secondary *Streptococcus pneumoniae* (*Spn*) infection. We observe that IAV synergistically sensitizes lung epithelial cells for PFT-mediated necroptosis *in vitro* and in murine models of *Spn* co-infection and secondary infection. Pharmacological induction of oxidative stress without virus sensitizes cells for PFT-mediated necroptosis. Antioxidant treatment or inhibition of necroptosis reduces disease severity during secondary bacterial infection. Our results advance our understanding on the molecular basis of co- and secondary bacterial infection to influenza and identify necroptosis inhibition and antioxidant therapy as potential intervention strategies.

Graphical Abstract

In Brief

Gonzalez-Juarbe et al. identify necroptosis as a pathway modulating disease severity during secondary bacterial infection (SBI) following influenza virus infection. They show that influenza-virus-induced oxidative stress is required to sensitize pulmonary cells to the pro-necroptotic activity of bacterial pore-forming toxins, providing a mechanism to explain the necrosis observed during SBI.

INTRODUCTION

Influenza A virus (IAV) is the most common cause of human influenza (flu) (Morens et al., 2008), infecting 4%–8% of the United States population annually (Tokars et al., 2018). Worldwide, the World Health Organization estimates that flu affects approximately 1 billion individuals annually, with 3 to 5 million cases of severe disease and a resulting 300,000 to 500,000 deaths (Clayville, 2011). IAV alone is capable of considerable morbidity and mortality, and clinical and molecular epidemiology have shown that the most serious infections are frequently associated with co-infections or a secondary infection with a bacterial pathogen. *Streptococcus pneumoniae* (*Spn*; the pneumococcus) is the leading cause of community-acquired pneumonia and by far the most common bacterium associated with IAV infections (van der Sluijs et al., 2010). Highlighting the seriousness of IAV/*Spn* co-infections, previous studies have shown that 34%–55% of the deaths linked to the 2009 IAV

pandemic were associated with bacterial infections, with *Spn* being the most common bacterium identified (Gill et al., 2010; Louie et al., 2009).

Over the past 20 years, many seminal discoveries have helped to explain, at the molecular level, the synergy observed during IAV/*Spn* super-infection. Key findings include the observation that IAV neuraminidase cleaves terminal sialic acid on host cell glycoconjugates, exposing normally cryptic antigens for bacterial attachment (McCullers and Bartmess, 2003). Viralneuraminidase-cleaved sialic acid serves as a nutrient for *Spn* and promotes bacterial outgrowth (Hentrich et al., 2016). IAV-induced downregulation of ion channels in bronchial epithelial cell results in dysregulated pulmonary fluid homeostasis that favors bacterial replication (Brand et al., 2018). Cytokines and alarmins released from IAV-infected dying cells elicit a transcriptional response from *Spn* that causes it to disperse from biofilms and enhances its virulence (Pettigrew et al., 2014). In addition, IAV-induced interferon (IFN) gamma downregulates the expression of scavenger receptors on macrophages, such as MARCO, that are required for uptake of *Spn* in the absence of a capsule-specific antibody (Sun and Metzger, 2008). Finally, the immune response induced by IAV is inappropriate for the clearance of bacteria and enhances pulmonary injury (Shahangian et al., 2009; van der Sluijs et al., 2006). It is noteworthy that most of this work has not focused on events that occur within lung epithelial cells (LECs), which are the nexus of co-infection.

Necroptosis is a programmed form of cell death that results in host cell membrane loss of integrity and cell lysis, i.e., necrosis. It is inflammatory due to the release of cytoplasmic contents that serve as alarmins. Canonically, necroptosis is regulated by receptor-interacting serine-threonine kinase 1 (RIPK1), which activates RIPK3. Subsequently, RIPK1/RIPK3 activates the necroptosis effector molecule MLKL through phosphorylation, p-MLKL, which targets cell membranes leading to cell rupture and death (Vandenabeele et al., 2010; Moreno-Gonzalez et al., 2016). Importantly, both IAV and bacterial pore-forming toxins (PFTs), such as pneumolysin produced by *Spn*, have recently been shown to induce necroptosis of LECs in a death-receptor-independent manner (González-Juarbe et al., 2017, 2018; Nogusa et al., 2016; Wang et al., 2019; Thapa et al., 2016). For IAV, this has been shown to be the result of viral RNA interactions with DNA-dependent activator of IFN regulatory factors (DAI) (also known as Zbp or DLM-1), a sensor for cytoplasmic nucleic acid, which activates RIPK3. Necroptosis of virally infected LECs is thought to be beneficial, as RIPK3 knockout (KO) and MLKL/FADD double-KO mice were considerably more susceptible to IAV, with the latter showing inhibited death of virus-infected cells. Along such lines, RIPK3 activation is necessary to establish an efficient response to the virus. (Nailwal and Chan, 2019; Nogusa et al., 2016; Balachandran and Rall, 2020). Our research group has shown that during bacterial pneumonia, initiation of necroptosis (i.e., MLKL-activity) is detrimental and exacerbates bacterial outgrowth, pulmonary injury, and loss of alveolar-capillary integrity (González-Juarbe et al., 2015a; González-Juarbe et al., 2017). Together, these observations suggest that inhibition of MLKL may have a possible protective role for viral and bacterial infections alike and extend to co-bacterial infections and secondary bacterial infections (SBIs). Critically and up to this point, the role of necroptosis on disease severity during IAV/bacterial co-infection was not known. Here, we

determined its consequence and identified IAV-induced oxidative stress as a sensitizing agent for PFT-mediated cell death.

RESULTS

Necroptosis Is Synergistically Increased during IAV/Spn Co-infection

Using an established mouse model of co-infection (McCullers and Hayden, 2012; McCullers and Tuomanen, 2001), we recapitulated the synergy known to occur between IAV and *Spn*. Briefly, we observed a >50-fold increase in the amount of *Spn* present in bronchoalveolar lavage fluid (BALF) and blood (Figures 1A and 1B), as well as a significant decrease in time to death following IAV/*Spn* challenge versus *Spn* or IAV alone (Figure 1C). Importantly, ongoing IAV infection synergistically enhanced the number of lung cells undergoing necroptosis after *Spn* challenge; necroptosis activity in frozen lung sections was inferred by immunofluorescent detection of p-MLKL (Figures 1D and 1E).

To validate this *in vivo* observation and to begin to dissect the molecular mechanisms underlying IAV-enhanced bacteria-induced necroptosis, we used an established *in vitro* co-infection model (Hoffmann et al., 2016). Briefly, A549 type II alveolar epithelial cells were infected with either pdmH1N1 or PR8 at a MOI of 2 for 2 h and then challenged with *Spn* at a MOI of 10 for another 4 h. Importantly, A549 cytotoxicity was synergistically increased in cells challenged with both pathogens (Figures 2A and 2B). Similar results were also observed with MH-S murine alveolar macrophages (Figure 2C), indicating influenza-mediated sensitization to necroptosis is not restricted to airway epithelial cells. Notably, the enhanced death of A549 co-infected cells occurred without significant differences in bacterial titers versus control (Figure S1A), indicating that the increased levels of necroptosis observed *in vivo* were not solely due to increased bacterial burden. Tumor necrosis factor (TNF) and IFN responses have been shown to promote necroptosis during viral infection (Upton et al., 2017). Along such lines, inhibition of TNF receptor 1 or blocking of TNF-α by pre-treatment of cells with R7050 or SPD304, respectively, did not reduce influenza-induced cell death potentiation in A549 cells *in vitro* (Figure S1B). Moreover, the time frame of the *in vitro* model did not lead to significant increases in the IFN response (Figure S1C). Altogether, our results show that there is no evidence supporting a role for the synergistic initiation of receptor-mediated apoptosis *in vitro* or *in vivo* under the conditions tested (Figure S2).

PFT Activity Is Required for *Spn*-Induced Necroptosis during Co-infection

Spn-mediated cytotoxicity of LECs was found to require the pore-forming activity of its PFT pneumolysin (Figures 2A and 2B). Furthermore, when A549 cells were treated with inhibitors of MLKL, necrosulfonamide (NSA) (Figure 2A), RIPK3, or GSK' 872 (Figure S3A), the enhanced sensitivity of these cells to *Spn* killing was lost. Challenge of IAV-infected A549 cells with recombinant pneumolysin (rPly) or α-toxin (the PFT of *Staphylococcus aureus*, the second most common isolate during SBIs to influenza; Morris et al., 2017), recapitulated the potentiation of cell cytotoxicity observed with live bacterial infection (Figure S3B–S3C). Potentiation of necroptosis by IAV was confirmed by immunoblot and immunofluorescent staining, which both showed enhanced amounts of p-

MLKL in A549 cells (Figures S3D–S3F). Further supporting a key role for necroptosis was the observation that A549 cells deficient in MLKL were protected against exacerbated PFT-mediated cell death after influenza infection (Figure 2C). Moreover, the same results were observed with primary normal human bronchiolar epithelial cells (nHBEs) *ex vivo* (Figure S3G). Together, our data provide evidence that necroptosis is the main contributor of cell necrosis during co- and secondary infection. Notably, caspase inhibition (Figure S2) did not confer significant protection, suggesting a smaller role for TLR and inflammasome signaling (apoptosis and pyroptosis) in the potentiation of cell death. In support of these results, we have previously demonstrated that pneumolysin alone leads to death-receptor-independent necroptosis in pulmonary epithelial cells (González-Juarbe et al., 2017).

IAV-Induced Oxidative Stress Sensitizes Cells *In Vitro* for PFT-Mediated Necroptosis

IAV-mediated oxidative stress has potent effects on pulmonary epithelial cells and the immune system (Liu et al., 2017). Therefore, it seemed plausible that the oxidative stress induced by the virus may be contributing toward the potentiation of pneumolysin-mediated necroptosis. In support of this notion, we observed that respiratory epithelial cells challenged *in vitro* with pdmH1N1 or PR8 showed increased levels of lipid peroxidation (Figure 3A; Figure S4A), as measured by malondialdehyde (MDA), and cellular reactive oxygen species (ROS) (Figure 3B; Figure S4B), as measured using cell-permeant 2', 7'-dichlorodihydrofluorescein diacetate (H2-DCF). Importantly, and despite not having an effect on viral titers during the course of infection (Figure 3C), pre-treatment of A549 cells with the su-peroxide dismutase mimetic Tempol (Brissac et al., 2017) before viral challenge reduced cell death and MLKL activation in co-infected cells (Figures 3D and 3E). Directly implicating oxidative stress as a primer for PFT-induced necroptosis, treatment of cells with paraquat (González-Juarbe et al., 2015a) enhanced the toxicity of rPly toward LECs, and the observed potentiating effect of paraquat was abolished by treatment with Tempol (Figure 3F). Identical results were observed using nHBEs *ex vivo* (Figure 3G) and were replicated by addition of exogenous H_2O_2 in place of paraquat to A549 epithelial cells prior to rPly challenge (Figure S4C). Note that *Spn* also produces H_2O_2 by its metabolic enzyme SpxB (Brissac et al., 2017). Yet, IAV potentiation of cell death was also observed in A549 cells challenged with *Spn* *spxB* (Figure S4D), indicating that the priming effect of viral-induced ROS was sufficient. Importantly, inhibition of ROS in A549 cells with rotenone + thallium trifluoroacetate (mitochondria-dependent ROS inhibitor), apocynin (nicotinamide adenine dinucleotide phosphate [NADPH]-dependent ROS inhibitor), allopurinol (xanthine-oxidase-dependent ROS inhibitor), or mefenamic acid (cyclooxygenase-dependent ROS inhibitor) all conferred protection against death caused by co-infection (Figure 3H). These results suggested that ROS potentiation of necroptosis may come from multiple cellular sources. Last, and to further probe the specificity of oxidative stress as a primer for necroptosis, we tested whether blockage of viral neuraminidase activity with oseltamivir (Takahashi et al., 2003) or treatment of cells with Pimodivir (VX-787) (Byrn et al., 2015), a non-nucleoside polymerase basic protein 2 subunit inhibitor, impacted cell death. Neither oseltamivir nor Pimodivir affected cell death (Figures S5A and S5B), even though viral titers were decreased by Pimodivir treatment (Figure S5C).

IAV-Induced Oxidative Stress Remains Beyond Viral Clearance and Maintains Susceptibility to Bacterial-Toxin-Mediated Necroptosis

We examined whether residual oxidative stress induced by IAV helped to explain the enhanced susceptibility to bacterial infection that occurs even after IAV is cleared, i.e., in a secondary infection model. Lung sections from pdmH1N1-challenged mice 10 days post-IAV infection showed considerable evidence of oxidative damage to DNA, as well as lipid peroxidation (immunofluorescence [IF] 8-hydroxydeoxyguanosine and 4-hydroxynonenal staining, respectively) (Helbock et al., 1999; Kruman et al., 1997) in pulmonary tissue (Figures 4A–4D). Notably, these mice were confirmed to not have detectable virus (Figure 4E). Similar to co-infection results (see Figure 1), if these mice were challenged with *Spn*, we observed a >100-fold increase in bacterial lung titers 2 days after *Spn* challenge (Figure 5A). This finding was concomitant with greater lung consolidation, immune cell infiltration (Figure S6), and substantially enhanced levels of lung necroptosis in co-infected mice versus those with *Spn* alone (Figures 5B–5D). Importantly, mice challenged with TIGR4 *ply* in our secondary infection model had MLKL activation levels and bacterial titers equivalent to our negative control, i.e., mice infected with wild-type TIGR4 but also receiving the necroptosis inhibitor Nec-1s (Figures 5E–5G; Figure S7). Furthermore, TIGR4 *ply*-challenged IAV-infected mice had decreased mortality versus controls (Figure 5H). Interestingly, Tempol treatment at 12 and 24 h post-*Spn* infection reduced the amount of necroptosis in the airway in our secondary IAV/*Spn* infection model, which happened despite Tempol not having an observed effect on *in vivo* levels of lipid oxidation (Figures 6A–6E). Tempol treatment also reduced bacterial burden within the airway of infected mice (Figure 6F). Thus, necroptosis sensitizing ROS is primarily due to the virus, persisted beyond detectable IAV infection, and acted directly to sensitize the cell for necroptosis.

In Vivo Necroptosis Inhibition Reduces the Severity of SBIs to Influenza

Although no changes in oxidative-stress-induced DNA damage were observed (Figures 7A and 7B), MLKL-deficient mice with secondary *Spn* infection had reduced bacterial titers, reduced lung consolidation, and a reduction in overall TUNEL-positive staining in lung sections (a general marker of cell death) (Figures 7C–7G). In addition, lungs of MLKL KO mice showed decreased levels of IFN-α and -β, suggesting a possible role for necroptosis in the IFN response during secondary infections (Figures 7H and 7I). Most importantly, MLKL KO mice had greater survival than the control mice in our secondary infection model (Figure 7J). Altogether, our results implicate oxidative-stress-enhanced PFT-mediated necroptosis activity as a major driver of disease severity and lung injury during co- and secondary infections to influenza.

DISCUSSION

The molecular mechanisms of IAV subversion of cellular defenses and programmed cell death continue to be investigated (Yeganeh et al., 2013; Balachandran and Rall, 2020). Only recently has it become apparent that necroptosis is essential for the control of virus replication during infection (Nogusa et al., 2016). Herein, we demonstrate that oxidative stress triggered by IAV infection plays a role in the potentiation of PFT-induced necroptosis in respiratory cells and thereby worsens injury. Furthermore, pharmacological blocking of

ROS from distinct sources conferred protection against IAV-induced sensitization to PFT-induced necroptosis.

Oxidative stress is pleiotropic and capable of oxidizing proteins and lipid membranes, damaging nucleic acids, and potentially altering cellular energy levels or ion homeostasis of the cell (Sies et al., 2017). The latter were shown to be triggers for non-canonical activation of necroptosis within bacteria-infected cells (González-Juarbe et al., 2015a, 2017, 2018). Importantly, in this study, increased susceptibility to PFT-mediated necroptosis was still observed even when IAV replication was blocked with Pimodivir. Moreover, Tempol-mediated protection against priming for PFT killing was applicable to both the co-infection and secondary infection scenario, namely, the latter when virus is no longer present. This suggests the mechanism responsible for IAV-mediated necroptosis potentiation is directly affected by acute intracellular ROS levels and is independent of viral replication. Whether and how the latter pathways are sensitized as a result of IAV-induced ROS or if an independent mechanism is responsible remains unclear, and detailed studies are now warranted to discern key similarities and differences between these events.

Necroptosis is inflammatory and therefore a "dual-edged sword" important for instigating a robust immune response, but it is also detrimental under conditions in which it is excessive (Yeganeh et al., 2013; Balachandran and Rall, 2020). Along such lines, sensitization to necroptosis most likely contributes to a variety of clinical problems during co- and secondary pneumonia marked by excessive inflammation, such as acute respiratory distress syndrome and sepsis, which are both a direct consequence of the enhanced level of cell death and release of pro-inflammatory alarmins. It is noteworthy that IAV has been specifically demonstrated to drive *Spn* development of otitis media (Tong et al., 2000), which is recognized to be a chronic inflammatory state. Critically, it is unknown if other viruses enhance permissiveness for PFT-mediated necroptosis, and this is an important avenue of future investigation. In support of this notion, a wide variety of viruses have been shown to induce oxidative stress in host cells by a variety of means (Schwarz, 1996). For example, respiratory syncytial virus does so by modulating levels of antioxidant enzymes (Hosakote et al., 2009) and has recently been shown to induce necroptosis in children and in a neonatal mouse model of infection (Simpson et al., 2020). Thus, it is likely that this phenomena is not restricted to IAV. Our prior published work (González-Juarbe et al., 2015a, 2017) and that with *S. aureus* α-toxin herein, which showed a wide variety of PFT-producing bacteria can instigate necroptosis of LECs, suggest viral-enhanced PFT-mediated necroptosis is not restricted to the pathogen *Spn.* Thus, this synergy may be an important contributor to enhanced disease severity at other anatomical sites in which virus and bacteria can co-infect.

Here, we demonstrate the critical role of pneumolysin in inducing cell necroptosis during secondary infections to influenza. Interestingly, Wolf et al. (2014) have shown that prior exposure of mice to a pneumolysin overexpressing *Spn* strain conferred protection against virus-induced morbidity and lung pathology. The authors concluded that immunity mounted against pneumolysin and its modulation of macrophage activity by arginase-1 reduce the severity of infection after re-challenge with pneumococcus and/or influenza infection. A recent publication by our group also demonstrated that pneumolysin induction of necroptosis

during bacterial colonization initiated low levels of inflammation required for the generation of an antibody-based response against *Spn* (Riegler et al., 2019). These findings suggest that the order in which the host is exposed to virus and bacteria has a profound impact on outcomes. Along such lines, McCullers and Rehg (2002) showed that *Spn* infection preceding IAV conferred protection against secondary bacterial challenge, whereas the reverse order of infection resulted in the dramatic sensitization to *Spn* that is studied herein. We now recognize IAV-induced susceptibility to necroptosis by oxidative stress as one contributing factor for this sequence-dependent sensitization.

Of note and during infection, other cells, particularly innate immune cells, also produce copious amounts of ROS (Chen et al., 2018), and they too may contribute to sensitization of LECs. Along such lines, To et al. (2020) recently showed that influenza infection promotes mitochondrial-derived ROS and that this in itself is detrimental to the lung epithelium, as measured by increased histopathological damage. Detailed studies are thereby required to better define the role of the bystander cells into these mechanisms as well as their own sensitivity to PFT-mediated killing during ROS production. Our results showing no differences in caspase activation suggest the responsible mechanism is also independent of canonical apoptotic and pyroptotic pathways, although it is likely these mechanisms are contributory to overall disease and occur in parallel during natural infection. This is in agreement with our previous observation that showed pneumolysin is able to initiate necroptosis in a death-receptor (TNFr and TLR4)-independent manner and that caspase activity may occur in parallel with necroptosis to modulate inflammation (González-Juarbe et al., 2017, 2018).

Finally, our results suggest that inhibition of the necroptosis pathway may be a viable therapeutic treatment during IAV-mediated co- or secondary infections, although the possibility remains that necroptosis inhibition may promote viral replication during co-infection, an aspect that needs to be studied (unpublished results with primary NHBEs suggest it does not). It is also important to consider that inhibition of RIPK1 and RIPK3 will have effects on aspects other than necroptosis, as the pathway is linked to apoptosis, nuclear factor κB (NF- κB) signaling, inflammation, and responses to ion changes (He and Wang, 2018). For this reason, targeting MLKL alone may be preferable, as it will not inhibit the ability of the cell to drive other responses beneficial against infection and reduce necrotic tissue damage and excess inflammation (Moreno-Gonzalez et al., 2016). Altogether, our results provide a molecular explanation for how influenza infection enhances permissiveness for SBIs. We demonstrate that PFT-mediated necroptosis is enhanced as a result of oxidative stress caused by prior or ongoing viral replications. Increased sensitivity to PFT-mediated necroptosis in turn worsens pulmonary damage and creates an environment that is further permissive for bacterial replication. The fact that oxidative stress induced by virus and PFT production are common across a wide range of viral and bacterial pathogens, respectively, suggests this is an important aspect of human infectious disease pathogenesis.

STAR★METHODS

RESOURCE AVAILABILITY

Lead Contact—Further information and requests for resources and reagents should be directed to and will be fulfilled by the Lead Contact, Dr.Gonzalez-Juarbe (ngonzale@jcvi.org).

Materials Availability—This study did not generate new unique reagents.

Data and Code Availability—This study did not generate/analyze datasets/code.

EXPERIMENTAL MODEL AND SUBJECT DETAILS

Ethics Statement—Animal experiments were approved by the Institutional Animal Care and Use Committee at The University of Alabama at Birmingham (Protocol # 20358). Human LEC were harvested from whole lung sections obtained from the International Institute for the Advancement of Medicine (Fulcher et al., 2005). The use of primary tissue, obtained in de-identified fashion, does not meet the criteria for human subject research.

IAV and Spn—Pandemic H1N1 A/California/7/2009 (pdmH1N1) and H1N1 A/Puerto Rico/8/1934 (PR8) influenza viruses were propagated in MDCK cells. *Spn* serotype 4 strain TIGR4 and its derivatives were used for all studies (Tettelin et al., 2001). TIGR4 mutants deficient in *ply* (*ply*), the gene encoding pneumolysin, and *spxB* (*spxB*), the gene encoding pyruvate oxidase, have been described (Lizcano et al., 2010). We also used mutants provided by Dr. Jeffrey Weiser (New York University, NY). These were matched strains of TIGR4 (TIGR4$_{JW}$), TIGR4 lacking pneumolysin, TIGR4$_{JW}$ *ply)*, a TIGR4 point mutant deficient in pore formation (TIGR4$_{JW}$ W433F), and a corrected mutant (TIGR4$_{JW}$ *ply*+) (Zafar et al., 2017); these were used as a set. Recombinant pneumolysin (rPly) was purified from *E. coli* (Brown et al., 2014). *Staphylococcus aureus* alpha-toxin was purchased (Sigma-Aldrich, St. Louis, MO).

Animal strains and infections—Male and female 8-week-old C57BL/6 mice were obtained from Taconic Biosciences (Rensselaer, NY). MLKL KO mice were made available by Dr. Warren Alexander (Walter and Eliza Hall Institute of Medical Research Parkville, Victoria, Australia) (Murphy et al., 2013). For IAV/*Spn* co-infection, 8-week-old C57BL/6 mice were intranasally challenged with 250 PFU PR8. Five days post-influenza challenge, mice received by forced aspiration 5×10^5 CFU *Spn* (González-Juarbe et al., 2015b). For the co-infection model we use an LD$_{50}$ of *Spn* to demonstrate bacterial infection was on its own capable of causing disease, yet this was augmented in a co-infection model. For studies involving *Spn* secondary infection, i.e., after viral clearance, mice were challenged with 250 PFU pdmH1N1 and ten days post-influenza, challenged with 10^3 CFU *Spn*. In all the secondary infection mouse models the *Spn* dose chosen was a sublethal (1000 CFU/mL) since the mice were challenged for 10-days with IAV, thus making the mice extremely susceptive to the bacterial infection (Gill et al., 2010; Louie et al., 2009).

Cell Infections—A549 type II alveolar epithelial cells (Fulcher et al., 2005), MH-S mouse alveolar macrophages (Saxena et al., 2008), and primary normal human bronchiolar epithelial cells (Fulcher et al., 2005), were infected with IAV at MOI 2 for 2 hours, and subsequently challenged with *Spn* at an MOI 10 for 4 hours. As our purpose was to characterize the cellular responses to influenza infection in regard to potentiation of bacteria induced cell death without the complication of cell lysis caused by late stage replication we used a high infectious dose and short time period. Other investigators have used the same approach (Hoffmann et al., 2016). The majority of chemical inhibitors were obtained from Sigma-Aldrich. Exceptions include necrosulfonamide (Tocris Bioscience, QL, UK), GSK'872 and Nec1s (BioVision, Milpitas, CA), oseltamivir carboxylate (MCE, Monmouth, NJ), TNFR inhibitor R-7050 and TNF-α inhibitor SPD-304 (Cayman Chemicals, Ann Arbor, MI) and Pimodivir (AdooQ Bioscience, Irvine, CA). Cells receiving inhibitors were treated continuously beginning 1-hour prior to IAV infection and inhibitor was maintained in the media until the end of the experiment. Pimodivir treated cells received the drug 2-hours prior to IAV challenge. A549 cells deficient in MLKL have been previously described (González-Juarbe et al., 2018). Cell death was evaluated by detection of lactate dehydrogenase (LDH) in culture supernatants (González-Juarbe et al., 2015a). The presence of reactive oxygen species (ROS) was measured with the H2-DCF assay (Thermo Fisher Scientific, Waltham, MA). Lipid peroxidation was detected with the lipid peroxidation malondialdehyde (MDA) assay (Abcam). Antibodies against 8-hydroxydeoxyguanosine, an oxidative stress-mediated DNA damage marker, and HNE-J, a lipid peroxidation marker, were purchased (Abcam).

METHOD DETAILS

Histology and Microscopy—The methods used for tissue processing, sectioning, and immunofluorescent microscopy are described (Gilley et al., 2016; González-Juarbe et al., 2015b, 2017). Briefly, tissue sections were fixed with cold acetone (−20°C), in 70% ethanol (−20°C). then rehydrated in PBS. The sections were then blocked \ in 3% goat serum–3% bovine serum albumin (BSA) for 30min. Each primary antibody used was diluted at 1:500 in the blocking solution and incubated over the tissue for 40 min. After incubation, sections were washed 3 times with PBS–0.05% Tween 20. Then sections were stained with secondary antibody diluted at 1:1000 in blocking solution and incubated over sections for 30 min. Slides were then washed 3 times and mounted with ProLong Gold Antifade reagent containing DAPI (4′,6′-diamidino-2-phenylindole) (Life Technologies, Carlsbad CA). For histology, formalin fixed slides were stained with hematoxylin, then washed, subsequently stained with eosin. Tissue was washed again and mounted with Cytoseal (ThermoFisher, Waltham, MA). Images were captured using a Zeiss AxioXam MRm Rev3 and/or MRc cameras attached to a Zeiss AxioImager Z1 epifluorescent microscope (Carl Zeiss, Thornwood, NY) or a Leica LMD6 with DFC3000G-1.3-megapixel monochrome camera (Leica Biosystems, Buffalo Grove, IL). TUNEL (Promega, Madison, WI) and Annexin V (Abcam, Cambridge, UK) staining was done per manufacturer's instruction. Cleaved caspase-3 staining was done using anti-cleaved-caspase-3 antibody (Abcam). Mean fluorescent intensity and densitometry of immunoblots was measured using ImageJ (Schindelin et al., 2015).

Immunoblots and ELISA—Western blots were done as previously described (Riegler et al., 2019). Briefly, 10 mg of total protein was separated on a 10% polyacryl-amide gel (Biorad) before transfer to a nitrocellulose membrane (Biorad). Membranes were blocked in 5% BSA and washed 3 times with TBS-0.1% Tween 20 (TBST). Membranes were incubated with anti -MLKL (1:1000, #37705, Cell Signaling Technologies), -p-MLKL (1:1000, #37333S, Cell Signaling Technologies) and -cytoskeletal actin (1:10000, #A300–485A, Bethyl Laboratories Inc., Montgomery, TX), in 5% BSA overnight. Then, membranes were washed 3 times with TBST and incubated with HRP-conjugated goat antibody at 1:10,000 (ThermoFisher, Waltham, MA). After 3 additional washes, signal was detected using Clarity Western ECL and ChemiDoc XRS+ (both from Biorad). ELISA-based measurements for IFN-β, IFN-α and TNF-α were done using kits from PBL Assay Science (Piscataway, NJ) and InvivoGen (San Diego, CA). For each cytokine, 100 μL of protein standard and supernatants of tissue homogenates were added to wells in a 96-well plate. Manufacturer instructions for washes and duration of detection antibody and HRP conjugate incubations were followed after initial sample incubation. Finally, absorbance or luminisence was read using a BioTek Synergy H4 plate reader (BioTek, Winooski, VT).

QUANTIFICATION AND STATISTICAL ANALYSIS

All results are displayed as standard error of the mean (SEM). In addition, individual data points in all *in vitro* assays represent all technical replicates collected from 3 separate experiments. For *in vivo* experiments, each individual data point represents an individual animal sample. Number of animals for *in vivo* experiments are denoted in the figure legends. For non-parametric multiple group analyses we used a Kruskal-Wallis H test with Dunn's post hoc analysis. For parametric grouped analyses we used ANOVA with Sidak's post hoc analysis. For data with a single independent factor of two groups we used a Mann-Whitney U test. Survival comparisons were assessed using Log-rank (Mantel-Cox) test. Asterisks denote the level of significance observed: * = $p \leq 0.05$; ** = $p \leq 0.01$; *** = $p \leq 0.001$; **** = $p \leq 0.0001$. Statistical analyses were calculated using Prism 8 (GraphPad Software: La Jolla, CA).

Supplementary Material

Refer to Web version on PubMed Central for supplementary material.

ACKNOWLEDGMENTS

REFERENCES

Balachandran S, and Rall GF (2020). Benefits and Perils of Necroptosis in Influenza Virus Infection. J. Virol 94, e01101–19. [PubMed: 32051270]

Brand JD, Lazrak A, Trombley JE, Shei RJ, Adewale AT, Tipper JL, Yu Z, Ashtekar AR, Rowe SM, Matalon S, and Harrod KS (2018). Influenza-mediated reduction of lung epithelial ion channel activity leads to dysregulated pulmonary fluid homeostasis. JCI Insight 3, e123467.

Brissac T, Shenoy AT, Patterson LA, and Orihuela CJ (2017). Cell invasion and pyruvate oxidase derived H2O2 are critical for Streptococcus pneumoniae mediated cardiomyocyte killing. Infect. Immun 86, e00569–17. [PubMed: 29061707]

Brown AO, Mann B, Gao G, Hankins JS, Humann J, Giardina J, Faverio P, Restrepo MI, Halade GV, Mortensen EM, et al. (2014). Streptococcus pneumoniae translocates into the myocardium and forms unique microlesions that disrupt cardiac function. PLoS Pathog. 10, e1004383. [PubMed: 25232870]

Byrn RA, Jones SM, Bennett HB, Bral C, Clark MP, Jacobs MD, Kwong AD, Ledeboer MW, Leeman JR, McNeil CF, et al. (2015). Pre-clinical activity of VX-787, a first-in-class, orally bioavailable inhibitor of the influenza virus polymerase PB2 subunit. Antimicrob. Agents Chemother 59, 1569–1582. [PubMed: 25547360]

Chen Y, Zhou Z, and Min W (2018). Mitochondria, Oxidative Stress and Innate Immunity. Front. Physiol 9, 1487. [PubMed: 30405440]

Clayville LR (2011). Influenza update: a review of currently available vaccines. P&T 36, 659–684. [PubMed: 22346299]

Fiore AE, Uyeki TM, Broder K, Finelli L, Euler GL, Singleton JA, Iskander JK, Wortley PM, Shay DK, Bresee JS, and Cox NJ; Centers for Disease Control and Prevention (CDC) (2010). Prevention and control of influenza with vaccines: recommendations of the Advisory Committee on Immunization Practices (ACIP). MMWR Recomm. Rep 59, 1–62.

Francis T (1935). Immunological relationships of strains of filterable virus recovered from cases of human influenza. Proc. Soc. Exp. Biol. Med 32, 1172–1175.

Fulcher ML, Gabriel S, Burns KA, Yankaskas JR, and Randell SH (2005). Well-differentiated human airway epithelial cell cultures. Methods Mol. Med 107, 183–206. [PubMed: 15492373]

Gill JR, Sheng ZM, Ely SF, Guinee DG, Beasley MB, Suh J, Deshpande C, Mollura DJ, Morens DM, Bray M, et al. (2010). Pulmonary pathologic findings of fatal 2009 pandemic influenza A/H1N1 viral infections. Arch. Pathol. Lab. Med 134, 235–243. [PubMed: 20121613]

Gilley RP, González-Juarbe N, Shenoy AT, Reyes LF, Dube PH, Restrepo MI, and Orihuela CJ (2016). Infiltrated Macrophages Die of Pneumolysin-Mediated Necroptosis following Pneumococcal Myocardial Invasion. Infect. Immun 84, 1457–1469. [PubMed: 26930705]

González-Juarbe N, Gilley RP, Hinojosa CA, Bradley KM, Kamei A, Gao G, Dube PH, Bergman MA, and Orihuela CJ (2015a). Pore-Forming Toxins Induce Macrophage Necroptosis during Acute Bacterial Pneumonia. PLoS Pathog. 11, e1005337. [PubMed: 26659062]

González-Juarbe N, Mares CA, Hinojosa CA, Medina JL, Cantwell A, Dube PH, Orihuela CJ, and Bergman MA (2015b). Requirement for Serratia marcescens cytolysin in a murine model of hemorrhagic pneumonia. Infect. Immun 83, 614–624. [PubMed: 25422267]

González-Juarbe N, Bradley KM, Shenoy AT, Gilley RP, Reyes LF, Hinojosa CA, Restrepo MI, Dube PH, Bergman MA, and Orihuela CJ (2017). Pore-forming toxin-mediated ion dysregulation leads to death receptor-independent necroptosis of lung epithelial cells during bacterial pneumonia. Cell Death Differ. 24, 917–928. [PubMed: 28387756]

González-Juarbe N, Bradley KM, Riegler AN, Reyes LF, Brissac T, Park SS, Restrepo MI, and Orihuela CJ (2018). Bacterial Pore-Forming Toxins Promote the Activation of Caspases in Parallel to Necroptosis to Enhance Alar-min Release and Inflammation During Pneumonia. Sci. Rep 8, 5846. [PubMed: 29643440]

He S, and Wang X (2018). RIP kinases as modulators of inflammation and immunity. Nat. Immunol 19, 912–922. [PubMed: 30131615]

Helbock HJ, Beckman KB, and Ames BN (1999). 8-Hydroxydeoxyguanosine and 8-hydroxyguanine as biomarkers of oxidative DNA damage. Methods Enzymol. 300, 156–166. [PubMed: 9919519]

Hentrich K, Löfling J, Pathak A, Nizet V, Varki A, and Henriques-Nor-mark B (2016). Streptococcus pneumoniae Senses a Human-like Sialic Acid Profile via the Response Regulator CiaR. Cell Host Microbe 20, 307–317. [PubMed: 27593514]

Hoffmann J, Machado D, Terrier O, Pouzol S, Messaoudi M, Basualdo W, Espínola EE, Guillen RM, Rosa-Calatrava M, Picot V, et al. (2016). Viral and bacterial co-infection in severe pneumonia triggers innate immune responses and specifically enhances IP-10: a translational study. Sci. Rep 6, 38532. [PubMed: 27922126]

Hosakote YM, Liu T, Castro SM, Garofalo RP, and Casola A (2009). Respiratory syncytial virus induces oxidative stress by modulating antioxidant enzymes. Am. J. Respir. Cell Mol. Biol 41, 348–357. [PubMed: 19151318]

Kruman I, Bruce-Keller AJ, Bredesen D, Waeg G, and Mattson MP (1997). Evidence that 4-hydroxynonenal mediates oxidative stress-induced neuronal apoptosis. J. Neurosci 17, 5089–5100. [PubMed: 9185546]

Liu M, Chen F, Liu T, Chen F, Liu S, and Yang J (2017). The role of oxidative stress in influenza virus infection. Microbes Infect. 19, 580–586. [PubMed: 28918004]

Lizcano A, Chin T, Sauer K, Tuomanen EI, and Orihuela CJ (2010). Early biofilm formation on microtiter plates is not correlated with the invasive disease potential of Streptococcus pneumoniae. Microb. Pathog 48, 124–130. [PubMed: 20096771]

Louie JK, Acosta M, Winter K, Jean C, Gavali S, Schechter R, Vugia D, Harriman K, Matyas B, Glaser CA, et al. (2009). Factors associated with death or hospitalization due to pandemic 2009 influenza A(H1N1) infection in California. JAMA 302, 1896–1902. [PubMed: 19887665]

McCullers JA, and Bartmess KC (2003). Role of neuraminidase in lethal synergism between influenza virus and Streptococcus pneumoniae. J. Infect. Dis 187, 1000–1009. [PubMed: 12660947]

McCullers JA, and Hayden FG (2012). Fatal influenza B infections: time to reexamine influenza research priorities. J. Infect. Dis 205, 870–872. [PubMed: 22291194]

McCullers JA, and Rehg JE (2002). Lethal synergism between influenza virus and Streptococcus pneumoniae: characterization of a mouse model and the role of platelet-activating factor receptor. J. Infect. Dis 186, 341–350. [PubMed: 12134230]

McCullers JA, and Tuomanen EI (2001). Molecular pathogenesis of pneumococcal pneumonia. Front. Biosci 6, D877–D889. [PubMed: 11502489]

Moreno-Gonzalez G, Vandenabeele P, and Krysko DV (2016). Necroptosis: A Novel Cell Death Modality and Its Potential Relevance for Critical Care Medicine. Am. J. Respir. Crit. Care Med 194, 415–428. [PubMed: 27285640]

Morens DM, Taubenberger JK, and Fauci AS (2008). Predominant role of bacterial pneumonia as a cause of death in pandemic influenza: implications for pandemic influenza preparedness. J. Infect. Dis 198, 962–970. [PubMed: 18710327]

Morris DE, Cleary DW, and Clarke SC (2017). Secondary Bacterial Infections Associated with Influenza Pandemics. Front. Microbiol 8, 1041. [PubMed: 28690590]

Murphy JM, Czabotar PE, Hildebrand JM, Lucet IS, Zhang JG, Alvarez-Diaz S, Lewis R, Lalaoui N, Metcalf D, Webb AI, et al. (2013). The pseudokinase MLKL mediates necroptosis via a molecular switch mechanism. Immunity 39, 443–453. [PubMed: 24012422]

Nailwal H, and Chan FK (2019). Necroptosis in anti-viral inflammation. Cell Death Differ. 26, 4–13. [PubMed: 30050058]

Nogusa S, Thapa RJ, Dillon CP, Liedmann S, Oguin TH 3rd, Ingram JP, Rodriguez DA, Kosoff R, Sharma S, Sturm O, et al. (2016). RIPK3 Activates Parallel Pathways of MLKL-Driven Necroptosis and FADD-Mediated Apoptosis to Protect against Influenza A Virus. Cell Host Microbe 20, 13–24. [PubMed: 27321907]

Pettigrew MM, Marks LR, Kong Y, Gent JF, Roche-Hakansson H, and Hakansson AP (2014). Dynamic changes in the Streptococcus pneumoniae transcriptome during transition from biofilm formation to invasive disease upon influenza A virus infection. Infect. Immun 82, 4607–4619. [PubMed: 25135685]

Riegler AN, Brissac T, Gonzalez-Juarbe N, and Orihuela CJ (2019). Necroptotic Cell Death Promotes Adaptive Immunity Against Colonizing Pneumococci. Front. Immunol 10, 615. [PubMed: 31019504]

Saxena RK, Gilmour MI, and Hays MD (2008). Isolation and quantitative estimation of diesel exhaust and carbon black particles ingested by lung epithelial cells and alveolar macrophages in vitro. Biotechniques 44, 799–805. [PubMed: 18476833]

Schindelin J, Rueden CT, Hiner MC, and Eliceiri KW (2015). The ImageJ ecosystem: An open platform for biomedical image analysis. Mol. Reprod. Dev 82, 518–529. [PubMed: 26153368]

Schwarz KB (1996). Oxidative stress during viral infection: a review. Free Radic. Biol. Med 21, 641–649. [PubMed: 8891667]

Shahangian A, Chow EK, Tian X, Kang JR, Ghaffari A, Liu SY, Belperio JA, Cheng G, and Deng JC (2009). Type I IFNs mediate development of postinfluenza bacterial pneumonia in mice. J. Clin. Invest 119, 1910–1920. [PubMed: 19487810]

Sies H, Berndt C, and Jones DP (2017). Oxidative Stress. Annu. Rev. Biochem 86, 715–748. [PubMed: 28441057]

Simpson J, Loh Z, Ullah MA, Lynch JP, Werder RB, Collinson N, Zhang V, Dondelinger Y, Bertrand MJM, Everard ML, et al. (2020). Respiratory Syncytial Virus Infection Promotes Necroptosis and HMGB1 Release by Airway Epithelial Cells. Am. J. Respir. Crit. Care Med 201, 1358–1371. [PubMed: 32105156]

Sun K, and Metzger DW (2008). Inhibition of pulmonary antibacterial defense by interferon-gamma during recovery from influenza infection. Nat. Med 14, 558–564. [PubMed: 18438414]

Takahashi K, Furuta Y, Fukuda Y, Kuno M, Kamiyama T, Kozaki K, Nomura N, Egawa H, Minami S, and Shiraki K (2003). In vitro and in vivo activities of T-705 and oseltamivir against influenza virus. Antivir. Chem. Chemother 14, 235–241. [PubMed: 14694986]

Tettelin H, Nelson KE, Paulsen IT, Eisen JA, Read TD, Peterson S, Heidelberg J, DeBoy RT, Haft DH, Dodson RJ, et al. (2001). Complete genome sequence of a virulent isolate of Streptococcus pneumoniae. Science 293, 498–506. [PubMed: 11463916]

Thapa RJ, Ingram JP, Ragan KB, Nogusa S, Boyd DF, Benitez AA, Sridharan H, Kosoff R, Shubina M, Landsteiner VJ, et al. (2016). DAI Senses Influenza A Virus Genomic RNA and Activates RIPK3-Dependent Cell Death. Cell Host Microbe 20, 674–681. [PubMed: 27746097]

To EE, Erlich JR, Liong F, Luong R, Liong S, Esaq F, Oseghale O, Anthony D, McQualter J, Bozinovski S, et al. (2020). Mitochondrial Reactive Oxygen Species Contribute to Pathological Inflammation During Influenza A Virus Infection in Mice. Antioxid. Redox Signal 32, 929–942. [PubMed: 31190565]

Tokars JI, Olsen SJ, and Reed C (2018). Seasonal Incidence of Symptomatic Influenza in the United States. Clin. Infect. Dis 66, 1511–1518. [PubMed: 29206909]

Tong HH, Fisher LM, Kosunick GM, and DeMaria TF (2000). Effect of adenovirus type 1 and influenza A virus on Streptococcus pneumoniae nasopharyngeal colonization and otitis media in the chinchilla. Ann. Otol. Rhinol. Laryngol 109, 1021–1027. [PubMed: 11089992]

Upton JW, Shubina M, and Balachandran S (2017). RIPK3-driven cell death during virus infections. Immunol. Rev 277, 90–101. [PubMed: 28462524]

van der Sluijs KF, Nijhuis M, Levels JH, Florquin S, Mellor AL, Jansen HM, van der Poll T, and Lutter R (2006). Influenza-induced expression of indoleamine 2,3-dioxygenase enhances interleukin-10 production and bacterial outgrowth during secondary pneumococcal pneumonia. J. Infect. Dis 193, 214–222. [PubMed: 16362885]

van der Sluijs KF, van der Poll T, Lutter R, Juffermans NP, and Schultz MJ (2010). Bench-to-bedside review: bacterial pneumonia with influenza -pathogenesis and clinical implications. Crit. Care 14, 219. [PubMed: 20459593]

Vandenabeele P, Galluzzi L, Vanden Berghe T, and Kroemer G (2010). Molecular mechanisms of necroptosis: an ordered cellular explosion. Nat. Rev. Mol. Cell Biol 11, 700–714. [PubMed: 20823910]

Wang Y, Hao Q, Florence JM, Jung BG, Kurdowska AK, Samten B, Idell S, and Tang H (2019). Influenza Virus Infection Induces ZBP1 Expression and Necroptosis in Mouse Lungs. Front. Cell. Infect. Microbiol 9, 286. [PubMed: 31440477]

Wolf AI, Strauman MC, Mozdzanowska K, Williams KL, Osborne LC, Shen H, Liu Q, Garlick D, Artis D, Hensley SE, et al. (2014). Pneumolysin expression by streptococcus pneumoniae protects colonized mice from influenza virus-induced disease. Virology 462–463, 254–265.

Yeganeh B, Rezaei Moghadam A, Tran AT, Rahim MN, Ande SR, Hashemi M, Coombs KM, and Ghavami S (2013). Asthma and influenza virus infection:focusing on cell death and stress

pathways in influenza virus replication. Iran. J. Allergy Asthma Immunol 12, 1–17. [PubMed: 23454774]

Zafar MA, Wang Y, Hamaguchi S, and Weiser JN (2017). Host-to-Host Transmission of Streptococcus pneumoniae Is Driven by Its Inflammatory Toxin, Pneumolysin. Cell Host Microbe 21, 73–83. [PubMed: 28081446]

Highlights

- IAV synergistically sensitizes pulmonary cells for PFT-mediated necroptosis

- Oxidative stress induced by IAV promotes PFT-mediated necroptosis

- Oxidative stress without virus sensitizes cells for PFT-mediated necroptosis

- Antioxidant treatment or necroptosis inhibition reduces disease severity during SBI
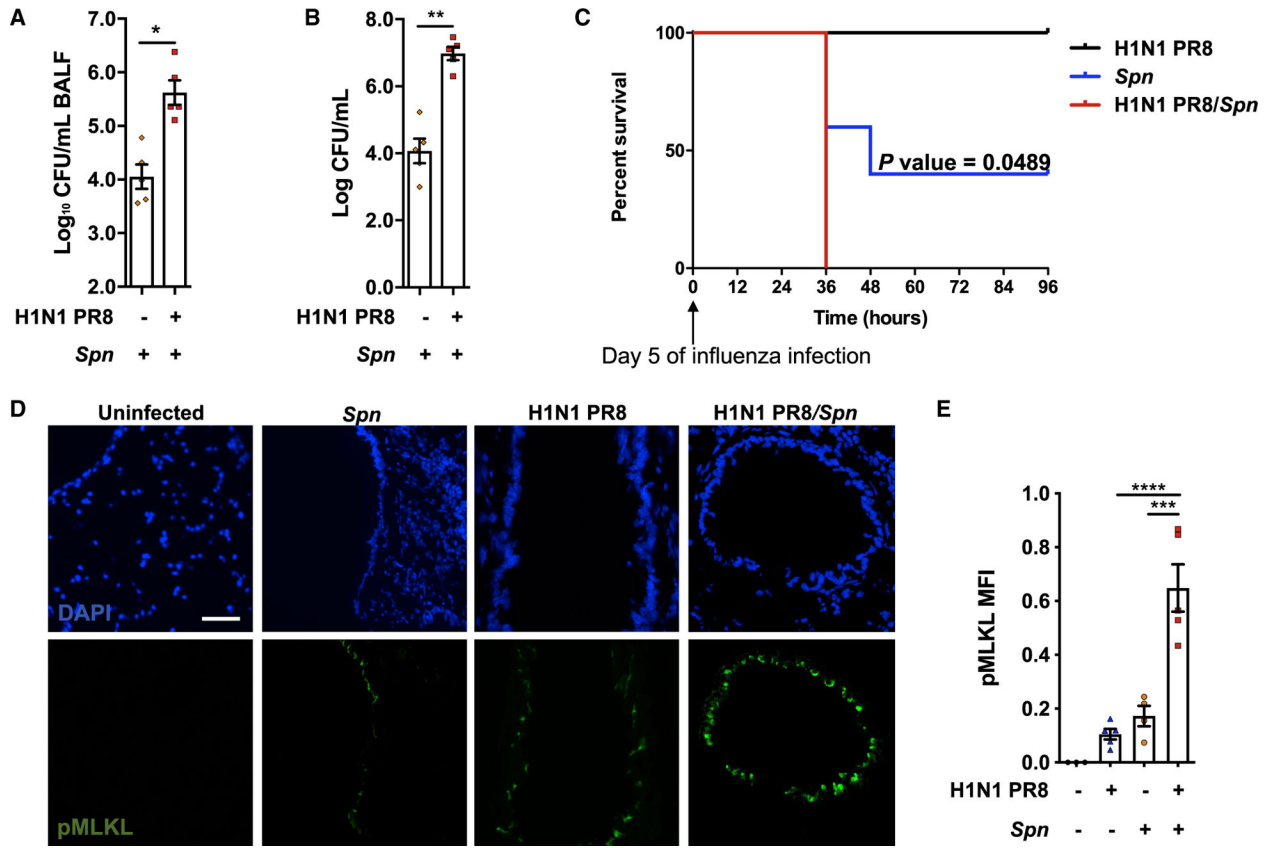
Figure 1. IAV/*Spn* Co-infection Leads to Increased Mortality and Enhanced Tissue Necroptosis
(A and B) Eight-week-old C57BL/6 mice were intranasally infected with H1N1 PR8 (250 plaque-forming units [PFUs]) for 5 days and subsequently challenged intratracheally with *Spn* strain TIGR4 at the lethal dose (LD$_{50}$) dose of 5×10^5 colony-forming units [CFUs]. Mice were euthanized 24 h post-secondary infection (n = 4–5 mice/cohort). Bacterial titers in bronchoalveolar lavage fluid (BALF) (A) and blood of mice at time of sacrifice (B).
(C) Survival of mice challenged with IAV, *Spn*, or co-infected with *Spn* after 5 days of IAV (n = 5).
(D) Corresponding and representative images of frozen lung sections from infected mice immunofluorescently stained for p-MLKL (green) (n = 4–5/cohort). White bar denotes 50 μm.
(E) Shown is the quantitation of p-MLKL levels in captured images calculated by mean fluorescent intensity (MFI). For *in vivo* experiments, each individual data point represents an individual animal sample.
Asterisks denote the level of significance observed: = P   0.05; *** = P   0.01; *** = P 0.001; **** = P   0.0001.
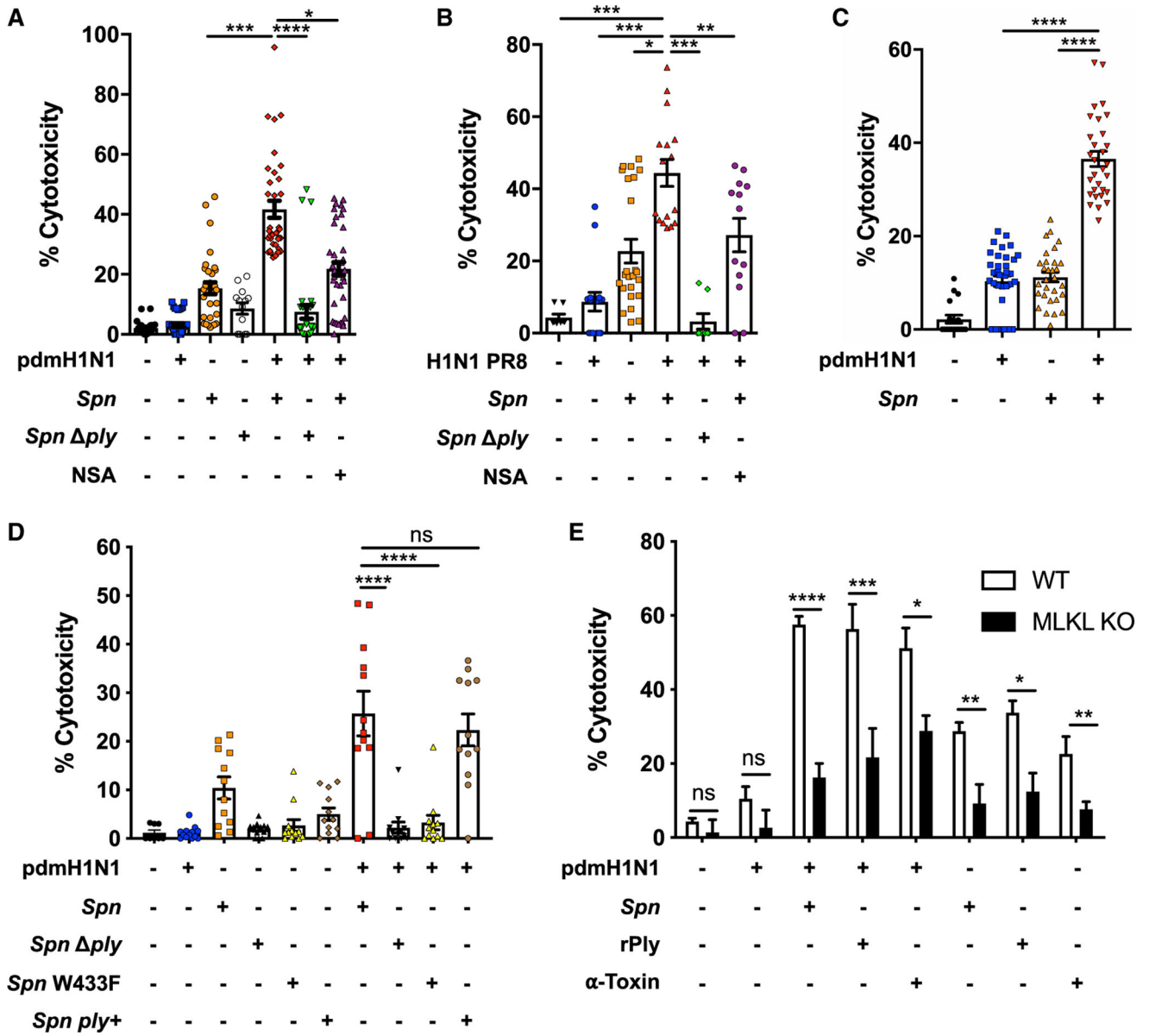
Figure 2. IAV Infection Promotes PFT-Mediated Cell Death

(A and B) Lactate dehydrogenase (LDH) release was measured from A549 cells following infection with influenza A/California/7/2009 (pdmH1N1) (A) and PR8 H1N1 (B) at a MOI of 2 for 2 h and challenge with wild-type *Spn* (*Spn*, in house strain) or Ply-deficient derivative (*Spn* ply) at an MOI of 10 for 4 additional h. Cells were treated with necrosulfonamide (NSA; 10 μM) when indicated.

(C) LDH release was measured from MH-S alveolar macrophages following an infection workflow as in (A).

(D) LDH cytotoxicity assay of supernatants from A549 cells was performed following infection with pdmH1N1 at an MOI of 2 for 2 h and challenge with *Spn* strains and mutants obtained from Dr. Jeffrey Weiser at an MOI of 10 for 4 h: (Zafar et al., 2017) *Spn* TIGR4

wild type (WT) (*Spn*), Ply-deficient mutant (*Spn* ply), Ply point mutant deficient in pore formation (*Spn* W433F), and corrected mutant (*Spn ply*+).

(E) Cytotoxicity of A549 WT (white bars) or A549 MLKL-deficient cells (black bars) was measured following the same challenge model as in (A) using *Spn*, recombinant pneumolysin (rPly), or alpha-toxin (α-Toxin). Individual data points in all *in vitro* assays represent all technical replicates collected from 3 separate experiments.

Asterisks denote the level of significance observed: * = P 0.05; ** = P 0.01; *** = P 0.001; **** = P % 0.0001.
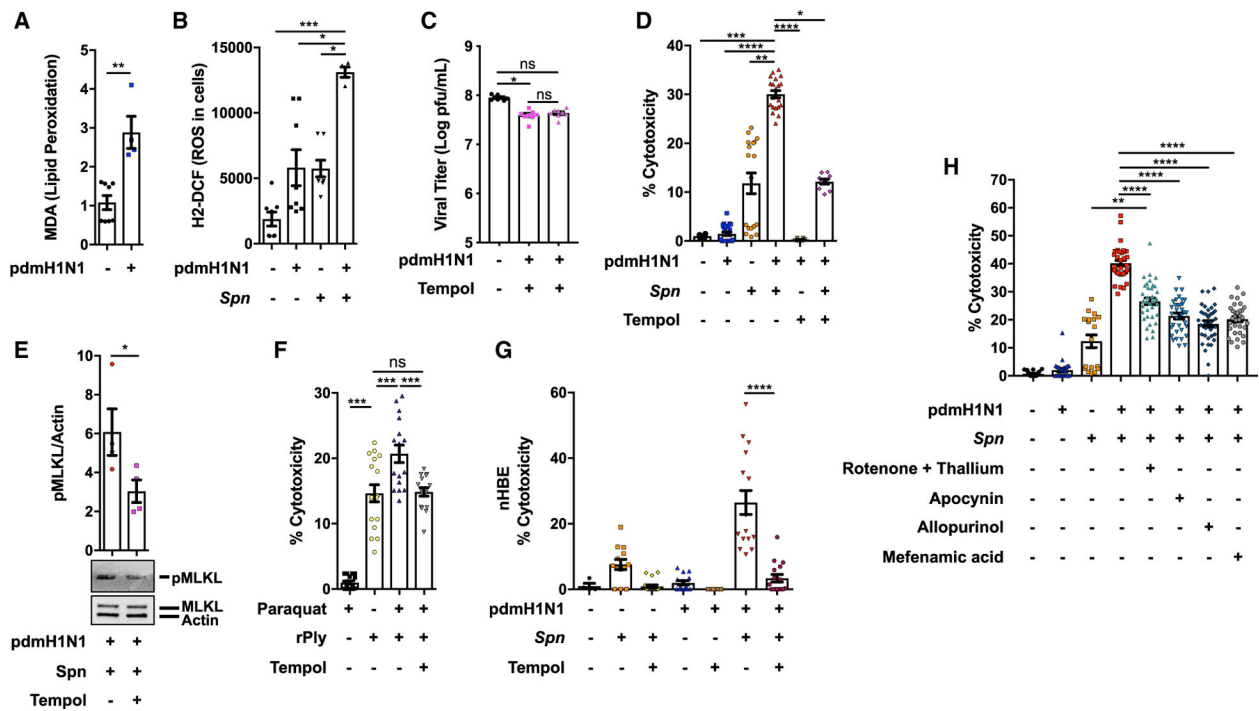
Figure 3. IAV-Mediated Oxidative Stress Potentiates Pneumolysin-Mediated Necroptosis

(A) Lipid peroxidation levels 4 h after challenge with pdmH1N1 were measured by MDA.

(B) Levels of cellular ROS measured in A549 cells infected with pdmH1N1 at a MOI of 2 for 2 h and then challenged with *Spn* at a MOI of 10 for 2 more h.

(C) Viral titers quantified (log PFU/mL) in A549 cells treated with Tempol (20 μM) for 1 h or 24 h.

(D and E) Cytotoxicity (E) and corresponding p-MLKL levels (F) in A549 cells were pre-treated with Tempol for 1 h, infected with pdmH1N1 at a MOI 2 for 2 h and then challenged with *Spn* at an MOI of 10 for 4 additional h.

(F) Cytotoxicity was measured in A549 cells pre-treated with Tempol and then treated with Paraquat (10 μM) for an additional 2 h, followed by challenge with rPly (0.1 μg) for 2 h.

(G) Cytotoxicity of *ex-vivo*-cultured primary normal human bronchial epithelial cells pre-treated with Tempol for 1 h, infected with pdmH1N1 at a MOI of 2 for 2 h, and challenged with *Spn* at an MOI of 10 for 4 additional h.

(H) LDH release from A549 cells pretreated with rotenone + thallium trifluoroacetate (10 nM/mL/10 nM/mL), a mitochondria-dependent ROS inhibitor; apocynin (1μM/mL), a NADPH-dependent ROS inhibitor; allopurinol (10 nM/mL), a xanthine oxidase-dependent ROS inhibitor; and mefenamic acid (20 nM/mL), a cyclooxygenase-dependent ROS inhibitor following IAV and *Spn*, individually and together. Individual data points in all *in vitro* assays represent all technical replicates collected from 3 separate experiments. Asterisks denote the level of significance observed: * = P   0.05; ** = P   0.01; *** = P   0.001; **** = P   0.0001.
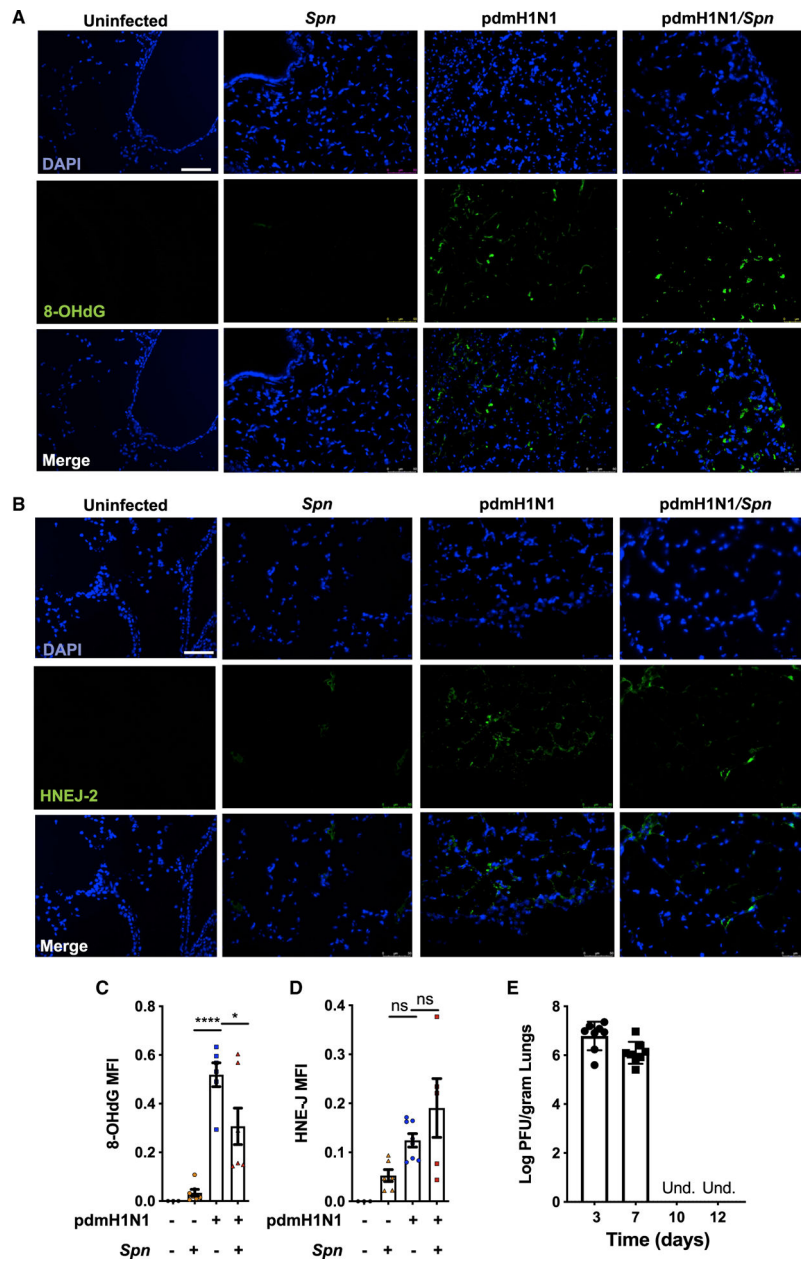
Figure 4. IAV-Mediated Oxidative Stress Persists after Virus Clearance *In Vivo*

(A and B) Eight-week-old C57BL/6 mice were intranasally infected with A/ California/7/2009 (pdmH1N1) and 10 days later challenged intratracheally with *Spn*. Mice were euthanized 48 h after secondary infection (n = 6–8 mice). Shown are representative immunofluorescent lung sections stained for 8-hydroxydeoxyguanosine (8-OHdG) (A) and 4-hydroxynonenal (HNE-J) (B). White bar denotes 50 μm.

(C and D) Quantification of the MFI of 8-OHdG and HNE-J stainings, respectively, was performed.

(E) Viral titers (log PFU/gram) in lungs at days 3, 7, 10, and 12 post-IAV infection (n = 8 mice per group) are indicated. For *in vivo* experiments, each individual data point represents an individual animal sample.

Asterisks denote the level of significance observed: * = P 0.05; ** = P 0.01; *** = P 0.001; **** = P 0.0001.
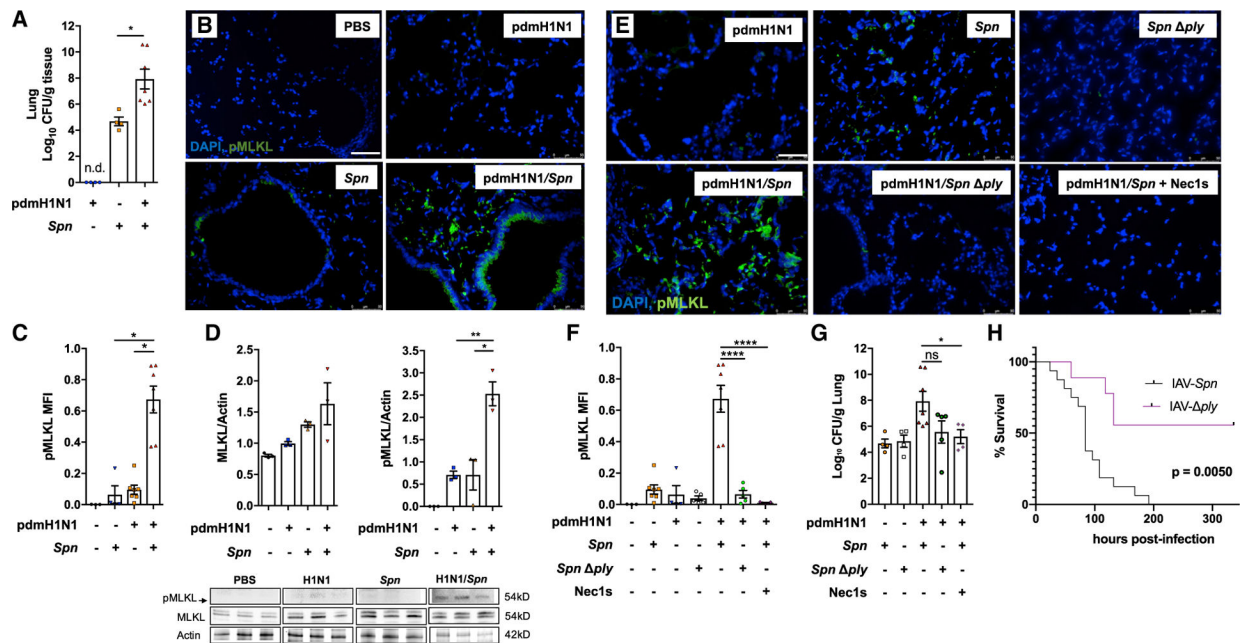
Figure 5. Influenza Infection Potentiates Pneumolysin-Induced Necroptosis Activation during Secondary *Spn* Challenge

(A and B) Eight-week-old C57BL/6 mice were intranasally infected with A/California/7/2009 (pdmH1N1) and 10 days later challenged intratracheally with *Spn*. Mice were euthanized 48 h after secondary infection (n = 3–7 mice). Shown are bacterial titers in homogenized lung samples (A), as well as representative images of corresponding lung sections stained for p-MLKL (3 sections stained per mouse) (B). White bar denotes 50 μm.

(C) MFI for p-MLKL activity was measured.

(D) Densitometry and western blots for p-MLKL, MLKL, and actin from mock-, *Spn*-, pdmH1N1-, and pdmH1N1/*Spn*-infected mice (n = 3/cohort).

(E–G) Eight-week-old C57BL/6 mice were intranasally infected with A/California/7/2009 (pdmH1N1) and 10 days later challenged intratracheally with *Spn* or *Spn* ply. Mice were euthanized 48 h after secondary infection (n = 4–7 mice). Treatment with Nec1s was done intraperitoneally at 12 and 24 h following bacterial challenge.

(E and F) Shown are representative images of lung tissue sections stained for p-MLKL (separate points are average of 3 pictures per mouse) (E) and MFI of pMLKL staining (F).

(G) Corresponding lung bacterial titers (CFU/g tissue) calculated.

(H) Survival of C57BL/6 mice following intranasal infection with pdmH1N1 for 10 days and subsequent intratracheal challenge with *Spn* or *Spn* ply were monitored. For *in vivo* experiments, each individual data point represents an individual animal sample.

Asterisks denote the level of significance observed: * = P   0.05; ** = P   0.01; *** = P   0.001; **** = P   0.0001.
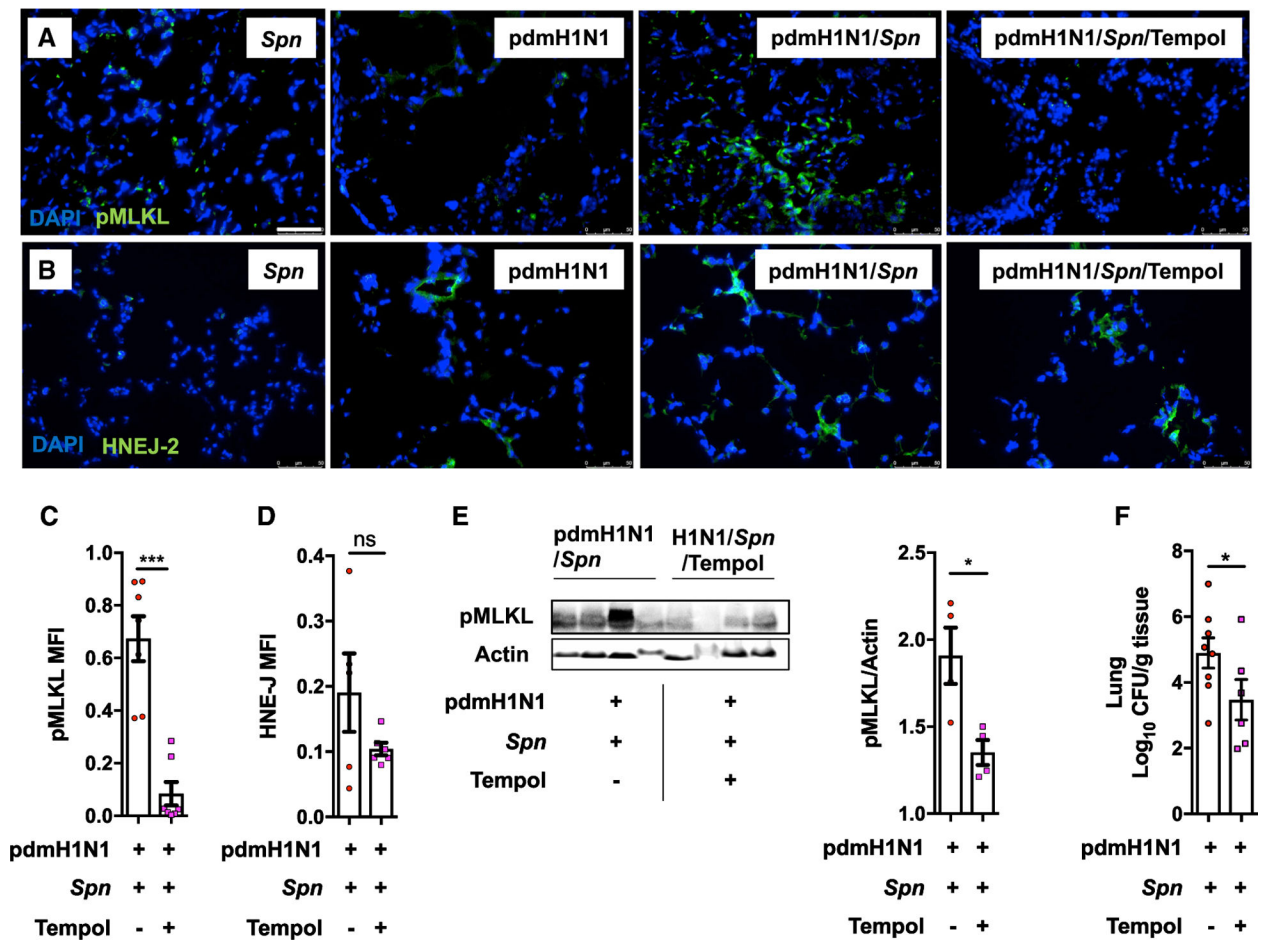
Figure 6. Therapeutic Neutralization of ROS Reduces Necroptosis Activation during Secondary Bacterial Pneumonia

(A and B) Eight-week-old C57BL/6 mice were intranasally infected with A/California/7/2009 (pdmH1N1) and 10 days later challenged intratracheally with *Spn*. Mice were euthanized 48 h after secondary infection (n = 5–8 mice). Tempol treatment was done intraperitoneally at 12 and 24 h post-bacterial infection. Representative images of lung sections immunofluorescently stained for p-MLKL (A) and HNE-J (B). White bar denotes 50 µm.

(C and D) Quantification of the MFI in corresponding captured images.

(E) Immunoblot for pMLKL and actin of pdmH1N1-infected mice, challenged with *Spn* with subsequent Tempol treatment, and its densitometry quantification.

(F) Bacterial titers measured in lungs at time of death. For *in vivo* experiments, each individual data point represents an individual animal sample. Asterisks denote the level of significance observed: * = P ≤ 0.05; ** = P ≤ 0.01; *** = P ≤ 0.001; **** = P ≤ 0.0001.
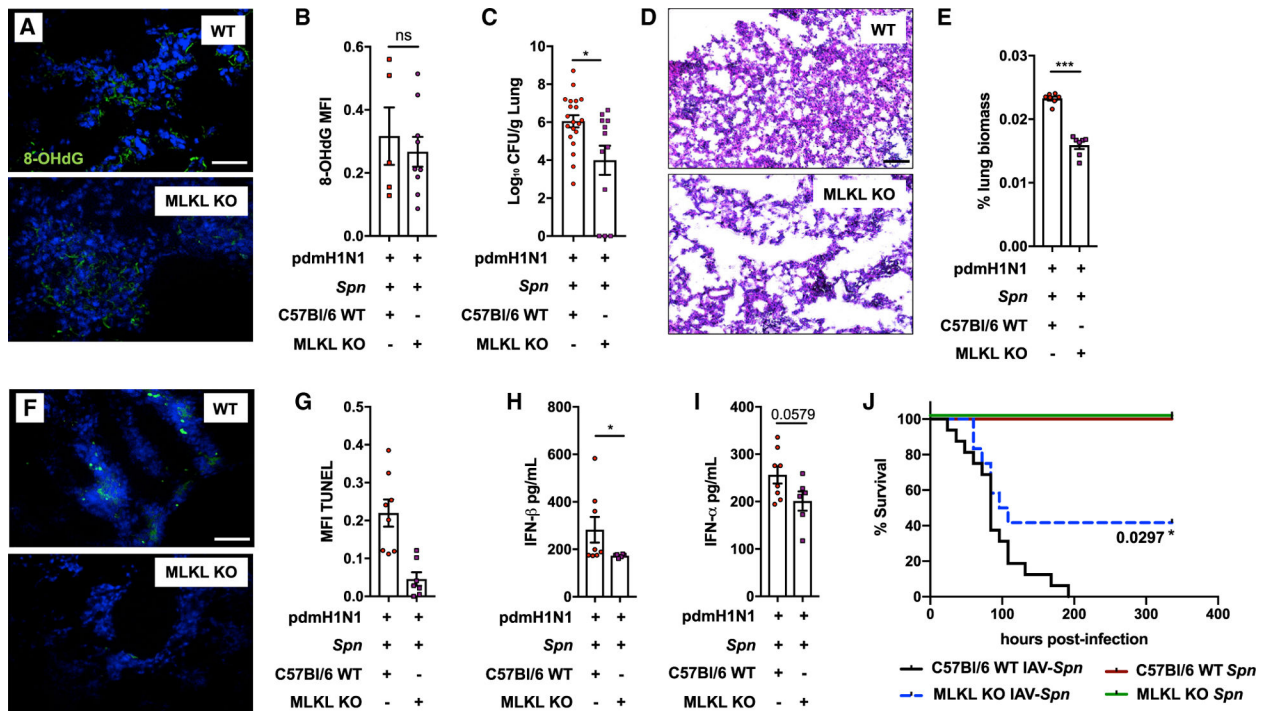
Figure 7. Inhibition of Necroptosis Reduces Disease Severity and Tissue Injury during Secondary Bacterial Pneumonia

Eight-week-old C57BL/6 mice were intranasally infected with A/California/7/2009 (pdmH1N1) and 10 days later challenged intratracheally with *Spn* (1,000 CFUs). Mice were euthanized 48 h after secondary infection (n > 12 mice).

(A) IF of 8-OHdG. White bar denotes 50 μm.

(B) Quantification of the MFI of 8-OHdG stainings.

(C) Measured bacterial titers in homogenized lungs.

(D) Representative H&E staining of corresponding tissue sections. Black bar denotes 100 μm.

(E) Lung consolidation in tissue sections, as measured using ImageJ (white space versus lung area, separate points are the average of 3 pictures per mouse). (F and G) TUNEL stain (white bar denotes 50μm)

(F) and MFI (G) of TUNEL stain quantified in lung sections.

(H and I) IFN-β (H) and (I) IFN-α levels (pg/mL) (I) in lung homogenates.

(J) Survival of 8-week-old WT and MLKL KO-C57BL/6 in the secondary *Spn* infection model (n = 8–12). For *in vivo* experiments, each individual data point represents an individual animal sample.

Asterisks denote the level of significance observed: * = P 0.05; ** = P 0.01; *** = P 0.001; **** = P 0.0001.

KEY RESOURCES TABLE

REAGENT or RESOURCE	SOURCE	IDENTIFIER
Antibodies		
8-hydroxydeoxyguanosine antibody	Abcam	#ab62623; RRID:AB_940049
HNE-J antibody	Abcam	#ab46545; RRID:AB_722490
MLKL antibody	Cell Signaling Technologies	#37705; RRID:AB_2799118
cleaved-caspase-3 antibody	Abcam	#ab49822; RRID:AB_868673
p-MLKL antibody	Cell Signaling Technologies	#37333S; RRID:AB_2799112
cytoskeletal actin antibody	Bethyl Laboratories Inc	#A300–485A; RRID:AB_451020
Bacterial and Virus Strains		
Pandemic H1N1 A/Califomia/7/2009	ATCC	Fiore et al., 2010
H1N1 A/Puerto Rico/8/1934 (PR8)	ATCC	Francis, 1935
Spn serotype 4 strain TIGR4	TIGR	Tettelin et al., 2001
TIGR4$_{JW}$	New York University	Zafar et al., 2017
TIGR4$_{JW}$ *ply*	New York University	Zafar et al., 2017
TIGR4$_{JW}$ W433F	New York University	Zafar et al., 2017
TIGR4$_{JW}$ *ply+*	New York University	Zafar et al., 2017
TIGR4 *ply*	UAB	Lizcano et al., 2010
TIGR4 *spxB*	UAB	Lizcano et al., 2010
Chemicals, Peptides, and Recombinant Proteins		
Necrosulfonamide	Tocris Bioscience	# 5025
GSK'872	BioVision	# 2673
Staphylococcus aureus alpha-toxin	Sigma-Aldrich	#H9395
hydrogen peroxide	Sigma-Aldrich	# 216763
catalase	Sigma-Aldrich	# C1345
oseltamivir carboxylate	MCE	#HY-13318
TNFR inhibitor R-7050	Cayman Chemicals	#16870
TNF-α inhibitor SPD-304	Cayman Chemicals	#869998-49-2
Pimodivir	AdooQ Bioscience	#A15993
Rotenone	Sigma-Aldrich	# 557368
Hematoxylin	Sigma-Aldrich	# H3136
Eosin	Sigma-Aldrich	# E4009
Thallium	Sigma-Aldrich	# T8266
Apocynin	Sigma-Aldrich	# 178385
Allopurinol	Sigma-Aldrich	# A8003
Mefenamic acid	Sigma-Aldrich	# M4267
Tempol	Sigma-Aldrich	#581500
Z-VAD-fmk	Tocris Bioscience	# 2163
Nec 1s	BioVision	#2263
Recombinant pneumolysin	UAB	Brown et al., 2014
Critical Commercial Assays		

REAGENT or RESOURCE	SOURCE	IDENTIFIER
Lactate dehydrogenase (LDH)	Thermo Fisher Scientific	#88954
H2-DCF assay	Thermo Fisher Scientific	#C6827
Malondialdehyde	Abcam	#ab118970
TUNEL	Promega	#G3250
IFN-β ELISA	PBL Assay Sci.	#42410–1
IFN-α ELISA	PBL Assay Sci.	#42120–1
TNF-α ELISA	R&D Systems	#MTA00B
Annexin V	Abcam, Cambridge, UK	#ab14085
Experimental Models: Cell Lines		
MLKL KO A549 cells	UAB	González-Juarbe et al., 2018
A549 cells	ATCC	CCL-185
MH-S mouse alveolar macrophages	ATCC	CRL-2019
Normal human bronchiolar epithelial cells	UAB	Fulcher et al., 2005
Experimental Models: Organisms/Strains		
C57BL/6	Taconic Biosciences	B6NTac
MLKL KO mice	Walter and Eliza Hall Institute of Medical Research Parkville, Victoria, Australia.	Murphy et al., 2013
Software and Algorithms		
ImageJ	NIH	https://imagej.nih.gov/ij/
Prism 8	GraphPad Software	https://www.graphpad.com:443/